A Trellis-Based Peak Frequency Tracking Technique for Photoplethysmographic Heart Rate Sensing during Exercise

Mizuki Kajita
Graduate School of Engineering
Osaka City University
Osaka, Japan
kajita@c.info.eng.osaka-cu.ac.jp

Yuzu Kuwahara
Graduate School of Engineering
Osaka City University
Osaka, Japan
kuwahara@c.info.eng.osaka-cu.ac.jp

Takunori Shimazaki
Sythesis Division
Soliton Systems K.K.
Osaka, Japan
takunori.shimazaki@soliton.co.jp

Shinsuke Hara
Graduate School of Engineering
Osaka City University
Osaka, Japan
hara@info.eng.osaka-cu.ac.jp

Hiroyuki Yomo
Graduate School of Science Engineering
Kansai University
Suita, Japan
yomo@kansai-u.ac.jp

Fumie Ono
Wireless Networks Research Center
NICT
Yokosuka, Japan
fumie@nict.go.jp

***Abstract*—We propose a novel trellis-based peak frequency tracking technique for photoplethysmographic (PPG) heart rate (HR) sensing. Dealing with HR changes on the time-frequency plane obtained by the Short Time-Discrete Fourier Transform as state transitions in a trellis diagram, the proposed technique rejects outliers induced during exercise. Experimental result involving thirteen subjects reveals that the proposed peak frequency tracking technique, which is combined with the recursive least squares algorithm-based MA cancellation technique, can achieve the root mean squares percent error of 6.924 % for a series of exercises with various intensities.**

I. Introduction

Heart rate (HR) sensing during exercise is essential for not only preventing disease and injury but also improving fitness, so nowadays, a variety of wearable devices for health care and sports purposes have been equipped with HR sensors. Among HR sensing methods, photoplethysmography (PPG) has been commonly used in these wearable devices, since it can simply, noninvasively and unobtrusively sense HR just by stabilizing a light emitting diode (LED) and a photo detector (PD) on the skin surface.

When a sensor wearer is stationary, since the set of LED and PD can be stabilized on his/her skin surface, the PD output contains only blood volume pulses (BVPs) in its alternating-current (AC) component. Consequently, PPG HR sensing works well. However, when he/she is exercising, since the thickness of his/her skin tissue changes and the set of LED and PD is likely to leave his/her skin surface according to his/her exercise, the PD output contains not only BVP component but also erroneous components such as motion artifact (MA) and outlier (OL). Consequently, PPG HR sensing becomes error-prone. For instance, it has been reported that the HR sensing error by PPG can be 20 beats per minute (bpm) on average and sometimes 40 bpm [1], [2].

There have been a number of techniques so far proposed for MA cancellation and OL rejection. Taking into consideration that the main frequency component of MA is the same as that of human body motion, TROIKA [3] cancels MA in the PPG output using the accelerometer output, and rejects OL by means of peak frequency tracking technique (PFT) which limits the HR search range within the neighbor of the previously estimated HR. In addition to TROIKA, focusing on the fact that when a set of LED and PD doest not contact the skin surface, the PD output contains only MA component so it can act as an MA sensor, the adaptive filter-based technique cancels MA in the PPG output using the MA sensor output [4], and rejects OL by accepting HR change within a pre-determined range [5]. We can see that OL rejection techniques play an essential role in PPG HR sensing, since only MA cancellation techniques cannot guarantee high HR sensing accuracy.

In this paper, we propose to extend the idea of PFT, which is applicable not directly to a normal PPG output which is rich in MA but to "a roughly MA canceled PPG output" after any MA cancellation technique. This paper is organized as follows. Section II explains the conventional peak frequency tracking technique. Section III presents the principle of the trellis-based peak frequency tracking technique. Section IV demonstrates and discusses experimental results. Finally, Section V concludes the paper.

This work was supported by the Research and Development of Innovative Network Technologies to Create the Future, the Commissioned Research of National Institute of Information and Communications Technology of Japan.

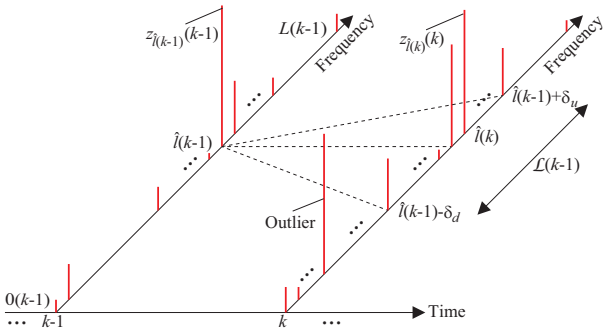

Fig. 1. Peak frequency tracking technique.

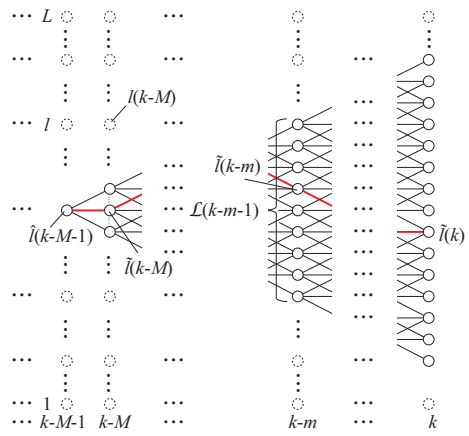

Fig. 2. Trellis diagram on the peak frequency tracking technique.

II. Conventional Peak Frequency Tracking Technique

First of all, we refer to "HR" in terms of not bpm but Hz simply as "frequency" in this paper.

Assuming that the sampling interval is T_s seconds, let us define the PPG output after an MA cancellation at the *i*th sampling instant as $x(i)$ $(i = 1, 2, \ldots)$. Then, $x(i)$ is expanded onto the time-frequency plane by the *L*-point Short Time-Discrete Fourier Transform (ST-DFT) where the frequency is estimated. Furthermore, assuming that the frequency is estimated every *K* samples, the ST-DFT output vector $(L \times 1)$ at the *k*th frequency estimation instant is written as

$$\begin{aligned} \mathbf{y}(k) &= [y_0(k), \ldots, y_l(k), \ldots, y_{L-1}(k)]^\top \\ &= \mathbf{F}_L \mathbf{W}_L \mathbf{x}(k) \qquad (1) \\ \mathbf{x}(k) &= [x(1 + K(k-1)), \ldots, \\ &\quad x(l + K(k-1)), \ldots, x(L + K(k-1))]^\top \qquad (2) \end{aligned}$$

where $(\cdot)^\top$ is the transpose of $(\cdot)$. In (1), $\mathbf{F}_L$ and $\mathbf{W}_L$ are the *L*-point ST-DFT and window matrices $(L \times L)$, respectively, which are defined as

$$\begin{aligned} \mathbf{F}_L &= \left\{ e^{-j2\pi \frac{(l_1-1)(l_2-1)}{L}} \right\}_{0 \le l_1, l_2 \le L-1} \qquad (3) \\ \mathbf{W}_L &= \mathrm{diag}\{w_0, \ldots, w_l, \ldots, w_{L-1}\} \qquad (4) \end{aligned}$$

where $\mathrm{diag}\{w_0, \ldots, w_l, \ldots, w_{L-1}\}$ is the diagonal matrix with $w_0, \ldots, w_l, \ldots, w_{L-1}$ as its main diagonal elements.

Defining the *k*th spectrogram, which is the *k*th amplitude vector $(L \times 1)$ for $\mathbf{y}(k)$, as

$$\begin{aligned} \mathbf{z}(k) &= [z_0(k), \ldots, z_l(k), \ldots, z_{L-1}(k)]^\top \\ &= [|y_0(k)|, \ldots, |y_l(k)|, \ldots, |y_{L-1}(k)|]^\top \qquad (5) \end{aligned}$$

the *k*th frequency is estimated as

$$\hat{l}(k) = \arg_l \max\{z_0(k), \ldots, z_l(k), \ldots, z_{L-1}(k)]\}. \qquad (6)$$

Figure 1 shows the conventional PFT. When $\hat{l}(k-1)$ is given, limiting the frequency transition from it, the conventional PFT estimates the *k*th frequency as

$$\begin{aligned} \hat{l}(k) &= \arg_l \max\{z_{\hat{l}(k-1)-\delta_d}(k), \ldots, z_{\hat{l}(k-1)}(k), \\ &\quad \ldots, z_{\hat{l}(k-1)+\delta_u}(k)]\} \qquad (7) \end{aligned}$$

where $\delta = -\delta_d, \ldots, -1, 0, +1, +\delta_u$ is the allowed frequency transition.

III. Trellis-Based Peak Frequency Tracking Technique

A. Principle

After the *k*th frequency has been estimated, the conventional PFT mentioned above considers the probability that the *k*th frequency is $l(k)$ as

$$p(l(k)) = \begin{cases} 1 & (l(k) = \hat{l}(k)) \\ 0 & (\text{otherwise}) \end{cases}. \qquad (8)$$

Borrowing a technical term in forward error correction (FEC) codes, the conventional PFT can be interpreted as making a "hard-decision" on the *k*th frequency. As in the case of decoding of FEC codes, we introduce a "soft-decision" into PFT.

Let us assume that now we have calculated the *k*th spectrogram $\mathbf{z}(k)$ but we have still estimated only up to the (*k*-*M*-1)th frequency as $\hat{l}(k-M-1)$ $(M = 0, 1, 2, \ldots)$. So the problem here is that we want to estimate the (*k*-*M*)th frequency using $\hat{l}(k-M-1)$, $\mathbf{z}(k-M)$, $\ldots$, $\mathbf{z}(k-m)$, $\ldots$, $\mathbf{z}(k)$. This is referred to as "filtering" for $M = 0$, which is equivalent to the conventional PFT, whereas "smoothing" for $M \ge 1$. Here, we refer to *M* as "the smoothing factor."

Figure 2 shows the trellis diagram on the peak frequency tracking technique, where the node labeled with $l(k)$ is the state that the *k*th frequency is $l(k)$ with probability of $p(l(k))$. Defining the route where the frequency starts from $\hat{l}(k-M-1)$, traverses through $\tilde{l}(k-M), \ldots, \tilde{l}(k-m), \ldots, \tilde{l}(k-1)$ and reaches $\tilde{l}(k)$ as

$$\begin{aligned} &r(k, \ldots, k-m, \ldots, k-M-1) \\ &\quad = \{(\tilde{l}(k), \tilde{l}(k-1)), \ldots, (\tilde{l}(k-m), \tilde{l}(k-m-1)), \\ &\qquad \ldots, (\tilde{l}(k-M), \hat{l}(k-M-1))\} \qquad (9) \end{aligned}$$

where $(\tilde{l}(k), \tilde{l}(k-1))$ is the link from $\tilde{l}(k-1)$ to $\tilde{l}(k)$, the occurrence probability of the route is given by the joint probability of the states as

$$\begin{aligned} & p(r(k, \ldots, k-m, \ldots, k-M-1)) \\ & = \quad p(\tilde{l}(k), \ldots, \tilde{l}(k-m), \\ & \qquad \ldots, \tilde{l}(k-M), \hat{l}(k-M-1)). \end{aligned} \tag{10}$$

In (10), assuming that the *k*th state probability depends only on the (*k*-1)th state probability, in other words, the frequency transition is modeled in a simple Markov process, taking $p(\hat{l}(k-M-1)) = 1$ into consideration, it can be decomposed into

$$\begin{aligned} & p(r(k, \ldots, k-m, \ldots, k-M-1)) \\ & = \quad \prod_{m=0}^{M} p(\tilde{l}(k-m) | \tilde{l}(k-m-1)). \end{aligned} \tag{11}$$

As in the case of the conventional PFT, when the frequency transition is limited, defining a set of the (*k*-*m*)th frequencies which can transit from $\tilde{l}(k-m-1)$ as

$$\begin{aligned} & \mathcal{L}(k-m-1) \\ & = \quad \{\tilde{l}(k-m-1)) + \delta |\ \delta = -\delta_d, \ldots, 0, \\ & \qquad \ldots, +\delta_u\} \end{aligned} \tag{12}$$

$p(\tilde{l}(k-m)|\tilde{l}(k-m-1))$ in (11) is approximated as

$$\begin{aligned} & p(\tilde{l}(k-m)|\tilde{l}(k-m-1)) \\ & = \quad q(\tilde{l}(k-m)) \end{aligned} \tag{13}$$

$$\approx \quad \begin{cases} p(\tilde{l}(k-m)) & (\tilde{l}(k-m) \\ & \in \mathcal{L}(k-m-1)) \\ 0 & (\text{otherwise}) \end{cases} . \tag{14}$$

Finally, defining a set of all the possible routes from $\hat{l}(k-M-1)$ to $\tilde{l}(k)$ as

$$\begin{aligned} & \mathcal{R}(k, \ldots, m, \ldots, k-M-1) \\ & = \quad \{r(k, \ldots, m, \ldots, k-M-1)| \\ & \qquad \tilde{l}(k-m) \in \mathcal{L}(k-m-1), \\ & \qquad m = 0, 1, \ldots, M, \\ & \qquad l(k-M-1) = \hat{l}(k-M-1)\} \end{aligned} \tag{15}$$

by substituting (14) into (11), the trellis-based PFT estimates

$$\begin{aligned} & \hat{l}(k-M) \\ & = \quad \arg_{\tilde{l}(k-M)} \max\{p(r(k, \ldots, k-M-1))| \\ & \qquad r(k, \ldots, k-M-1) \\ & \qquad \in \mathcal{R}(k, \ldots, k-M-1)\} \end{aligned} \tag{16}$$

$$\begin{aligned} & = \quad \arg_{\tilde{l}(k-M)} \max\{ \prod_{m=0}^{M-1} q(\tilde{l}(k-m))| \\ & \qquad \tilde{l}(k-m) \in \mathcal{L}(k-m-1), m = 0, \ldots, M\}. \end{aligned} \tag{17}$$

TABLE I
SPECIFICATIONS OF EXPERIMENTAL DEVICES.

Device	Specification
HR sensor	Size: 45 mm×44 mm×45 mm Weight: 31 grams Sampling interval: 0.1 seconds HR estimation interval: 1.0 second ST-DFT window width: 256 points Window functoin: Hanning Wireless: 920 MHz band, 100 kbps, 20 mW
Holter monitor	Fukuda FM120
Pressure gauge	AMI-Tech A0101-G35-AC
Treadmill	Horizon Citta T82

TABLE II
SUBJECT CHARACTERISTICS.

Number	13
Gender	Male
Age range	22-24
Height range	160-183 cm
Weight range	53-85 kilograms

TABLE III
DETAIL OF THE EXERCISES.

Speed (km/h)	0	4	0	6	0	8	0	10	0	12
Time period (min)	1	2	1	2	1	2	1	2	1	2

TABLE IV
SPECIFICATIONS OF THE TRELLIS-BASED PEAK FREQUENCY TRACKING WITH THE RLS-BASED MA CANCELLATION.

Smoothing factor (*m*)	Optimum parameters			
	N	λ	δ_d	δ_u
0	10	0.999	2	1
1	4	0.99	3	2
2	16	0.99	1	1
3	2	0.999	1	1

B. A Function for State Probability

To use (17), we need to know $q(l(k))$, that is, $p(l(k))$ $(l = 0, 1, \ldots, L-1)$, but it is generally unknown. Therefore, we need to assume a function for $q(l(k)) = f(\mathbf{z}(k))$. If the amplitude of a frequency component of $\mathbf{z}(k)$ is larger, the state probability of the frequency is higher, so it is reasonable that $p(l(k))$ is a monotonous increasing function of $z_l(k)$, so we assume the following polynomial function:

$$p_{poly}(l(k)) = \frac{z_l(k)}{\sum_{l=0}^{L-1} z_l(k)} \tag{18}$$

which is simply proportional to $z_l(k)$. Note that from (17), the estimation metric is given by the product of $p(l(k))$'s, so even if $z_l(k)$ is replaced by $z_l(k)^n$ $(n = 2, 3, \ldots)$, the magnitude correlation among the metrics does not change.

IV. EXPERIMENTAL RESULTS AND DISCUSSIONS

We conducted experiments involving 13 healthy male subjects. Their ages, heights, weights and BMIs ranged in 22-24, 160-183cm, 53-85kg and 19.4-25.4, respectively. Note that the experimental procedure was approved by the Institutional Review Board of Osaka City University.

As the PPG HR sensor, we used the wireless vital sensor [6], which was originally developed for real-time vital information monitoring for a group of exercisers. We put the PPG HR

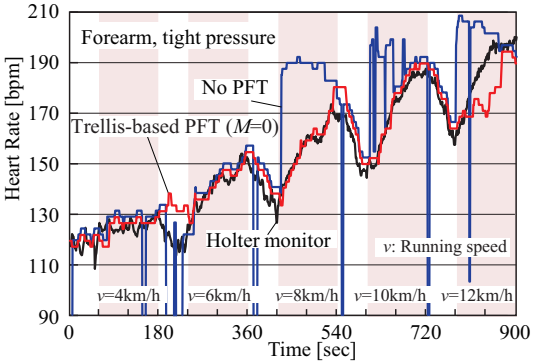

(a) Effect of filtering

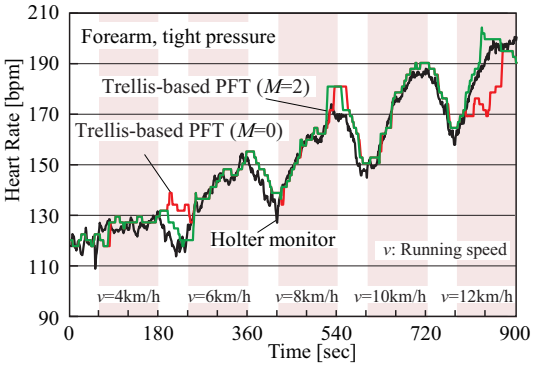

(b) Effect of smoothing

Fig. 3. Heart rate time variation for a subject.

sensor with an elastic belt to the forearm position of a subject, and a Holter monitor to the chest of the subject at the same time. According to the results in [7], we set the wearing pressure of "tight" to 50 hPa. We used the HR obtained by the Holter monitor as the reference.

The exercise protocol was composed of 1 min-standing rest, 2 min-walk (4 km/h), 1 min-standing rest, 2 min-fast walk (6 km/h), 1 min-standing rest, 2 min-jog (8 km/h), 1 min-standing rest, 2 min-run (10 km/h), 1 min-standing rest, and 2 min-fast run (12 km/h). When the subject was making a series of the exercises, we stored the data transmitted from the PPG HR sensor.

We processed the data in an off-line manner. For the MA cancellation, we adopted the technique using the MA sensor [4] based on a recursive least squares (RLS) algorithm [8] with two tunable parameters of the tap length (N) and forgetting factor (λ). For $M = 0, 1, 2, 3$, we optimized parameters to make the sensed HR error minimal.

Finally, Table I, II, III and IV summarize the specifications of the experimental devices, characteristics of subjects, exercise protocol, and specifications of the trellis-based peak frequency tracking with the RLS-based MA cancellation technique, respectively.

Figures 3 (a) and (b) show the HR time variation for a subject highlighting the effects of filtering ($M = 0$) and smoothing ($M = 2$) in the trellis-based PFT, respectively. We

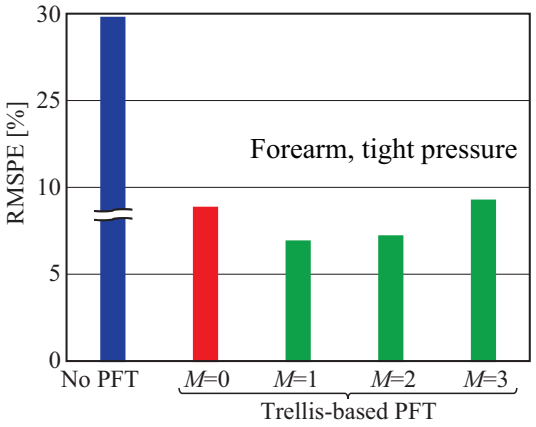

Fig. 4. RMSPE of the trellisb-based PFT.

can see from Fig. 3 (a) that without PFT, namely, just with PPG and MA cancellation technique, a lot of outliers occur in the estimated HR, whereas with the trellis-based filtering PFT, namely, $M = 0$, which is equivalent to the conventional PFT, these outliers are well rejected. In addition, we can see from Fig. 3 (b) that even with the trellis-based filtering PFT, namely, $M = 0$, which utilizes the past-to-present information on the PPG output, some errors still occur in the estimated HR, whereas with the trellis-based smoothing PFT, namely, $M = 2$, which utilizes the past-to-future-through-present information on the PPG output, these errors are well suppressed.

Finally, Figure 4 compares the root mean square percent error (RMSPE) of the trellis-based PFT with respect to the HR obtained by the Holter monitor. We can see from this figure that the RMSPE improves as the smoothing factor increases from $M = 0$ to $M = 1$, achieving the RMSPE of 6.924 %, but the RMSPE deteriorates as the smoothing factor further increases from $M = 1$ to $M = 3$. This is because a larger M means a longer observation period for the PPG output, so the occurrence probability of outlier increases in the longer observation period, which prevents the proposed PFT from selecting a correct HR route on the trellis.

V. Conclusion

In this paper, we have proposed a novel trellis-based peak frequency tracking technique (PFT) for photoplethysmographic (PPG) heart rate (HR) sensing. The trellis-based smoothing PFT outperforms the conventional filtering PFT achieving the RMSPE of 6.924 %, but longer smoothing periods do not always improve the HR estimation accuracy.

The mapping from the spectrogram to the probability is generally unknown, so to consider a more-suited function for it is included in our future works.

Acknowledgment

The research was supported by the Research and Development of Innovative Network Technologies to Create the Future, the Commissioned Research of National Institute of Information and Communications Technology (NICT) of Japan.

REFERENCES

[1] S. Gillinov, *et al.*, "Variable accuracy of wearable heart rate monitors during aerobic exercise," *Med Sci Sports Exerc.*, vol. 49, no. 8, pp. 1697-1703, 2017.

[2] R. Wang, *et al.*, "Accuracy of wrist-worn heart rate monitors," *JAMA Cardiol.*, vol. 2, no. 1, pp. 104-106, 2017.

[3] Z. Zhang, Z. Pi, and B. Liu, "TROIKA: A General Framework for Heart Rate Monitoring Using Wrist-Type Photoplethysmographic Signals During Intensive Physical Exercise," *IEEE Trans. on Biomed. Eng.*, vol. 62, no. 2, pp. 522-531, Feb. 2015.

[4] T. Shimazaki and S. Hara, "Cancellation of motion artifact induced by exercise for PPG-based heart rate sensing," *Proc. IEEE EMBC 2014*, pp. 3216-3219, Chicago, USA, 26-30 Aug. 2014.

[5] T. Shimazaki, *et al.*, "Motion artifact cancellation and outlier rejection for a clip-type PPG based heart rate sensor," *Proc. IEEE EMBC 2015*, pp. 2026-2029, Milan, Italy, 25-29 Aug. 2015.

[6] T. Hamagami, *et al.*, "Wireless multi-hop networking for a group of exercisers spread in a sports ground," *Proc. IEEE Healthcom 2018*, in CD-ROM, Ostrava, Czech, 17-20 Sep. 2018.

[7] T. Shimazaki, *et al.*, "Effect of position and fastening belt pressure on the accuracy of PPG-based heart rate sensor," *Proc. IEEE EMBC 2018*, pp. 4323-4326, Honolulu, Hawaii, 17-20 July. 2018.

[8] S. Haykin, *Adaptive Filter Theory, 4th ed,* Prentice-Hall, 2002.